eNOS Overexpression Exacerbates Vascular Closure in the Obliterative Phase of OIR and Increases Angiogenic Drive in the Subsequent Proliferative Stage

Kevin Edgar,[1] *Thomas A. Gardiner,*[1] *Rien van Haperen,*[2] *Rini de Crom,*[2] *and Denise M. McDonald*[1]

Purpose. In ischemic retinopathies, the misdirection of reparative angiogenesis away from the hypoxic retina leads to pathologic neovascularization. Thus, therapeutic strategies that reverse this trend would be extremely beneficial. Nitric oxide (NO) produced by endothelial nitric oxide synthase (eNOS) is an important mediator of vascular endothelial growth factor (VEGF) function facilitating vascular growth and maturation. However, in addition to NO, eNOS can also produce superoxide (O_2^-), exacerbating pathology. Here, our aim was to investigate the effect of eNOS overexpression on vascular closure and subsequent recovery of the ischemic retina.

Methods. Mice overexpressing eNOS-GFP were subjected to oxygen-induced retinopathy (OIR) and changes in retinal vascularization quantified. Background angiogenic drive was assessed during vascular development and in aortic rings. NOS activity was measured by Griess assay or conversion of radiolabeled arginine to citrulline, nitrotyrosine (NT), and superoxide by immunolabeling and dihydroethidium fluorescence and VEGF by ELISA.

Results. In response to hyperoxia, enhanced eNOS expression led to increased NOS-derived superoxide and dysfunctional NO production, NT accumulation, and exacerbated vessel closure associated with tetrahydrobiopterin (BH_4) insufficiency. Despite worse vaso-obliteration, eNOS overexpression resulted in elevated hypoxia-induced angiogenic drive, independent of VEGF production. This correlated with increased vascular branching similar to that observed in isolated aortas and during development. Enhanced recovery was also associated with neovascular tuft formation, which showed defective NO production and increased eNOS-derived superoxide and NT levels.

Conclusions. In hyperoxia, reduced BH_4 bioavailability causes overexpressed eNOS to become dysfunctional, exacerbating vaso-obliteration. In the proliferative phase, however, eNOS has important prorepair functions enhancing angiogenic growth potential and recovery in ischemia. (*Invest Ophthalmol Vis Sci.* 2012;53:6833–6850) DOI:10.1167/iovs.12-9797

Intravitreal neovascularization (NV) is a serious complication of several major retinal diseases, including diabetic retinopathy, retinopathy of prematurity, and retinal vein occlusion with uncontrolled vessel growth resulting in severe vision loss.[1–3] NV occurs in response to tissue ischemia and vascular endothelial growth factor (VEGF) stimulation; however, in the retina, new vessels often fail to recover the ischemic tissue and instead infiltrate the transparent vitreous resulting in visual impairment.[4,5] Current treatment regimens such as pan retinal laser photocoagulation, although effective, have significant side effects. Newer options designed to inhibit VEGF production decrease NV formation, but do not correct the underlying hypoxic stimulus, meaning that repeated administration is essential. Furthermore, because VEGF plays an important role in retinal endothelial and neuronal cell survival long term these treatments may not be ideal and may be potentially deleterious.[6] Together, the limitations of the current treatment regimens emphasize the importance of developing methods that inhibit the proangiogenic stimulus while also achieving a long-lasting therapeutic effect. One such alternative option could be to redirect new vessel growth into the hypoxic retina that would repair the ischemic retina while also preventing the growth of vessels into the vitreous.[7,8] To achieve this important goal it is important to understand the key regulators of angiogenesis in the unique tissue setting of the retina.

Angiogenesis in the retina is controlled largely by VEGF and there is now a considerable amount of evidence demonstrating that the angiogenic effect of VEGF is mediated, in part, through endothelial nitric oxide synthase (eNOS)–derived nitric oxide acting as a survival factor for endothelial cells by both suppressing apoptosis and promoting endothelial cell migration and tube formation.[9–14] Accordingly, increasing eNOS expression has been shown to have restorative potential for wound healing and angiogenesis in ischemia.[15,16]

In the eye the spatial orientation of the retinal vascular bed is critical to preserve the avascularity of the vitreous while also facilitating its role in maintaining tissue oxygenation and nutrient supply.[17,18] Thus, although it is known from studies on knockout animals that eNOS-derived nitric oxide is important to stimulate hypoxia-induced vascular growth, its role in promoting intraretinal versus intravitreal angiogenesis is unclear.[13] Nitric oxide is produced from arginine by three different isoforms of nitric oxide synthase and according to the amount produced and its cellular source, it may have either proangiogenic or paradoxically antiangiogenic actions. In the ischemic retina it has previously been shown that NO derived by inducible NOS is upregulated in glial cells in the avascular tissue during hypoxia,

From the [1]Centre for Vision and Vascular Science, Queen's University Belfast, Belfast, United Kingdom; and the [2]Department of Cell Biology and Genetics, Erasmus University Medical Centre Rotterdam, Rotterdam, The Netherlands.

Supported by Wellcome Trust UK and the Department for Employment and Learning (Northern Ireland).

Submitted for publication March 7, 2012; revised July 20, 2012; accepted August 20, 2012.

Disclosure: **K. Edgar**, None; **T.A. Gardiner**, None; **R. van Haperen**, None; **R. de Crom**, None; **D.M. McDonald**, None

Corresponding author: Denise M. McDonald, Centre for Vision and Vascular Science, Queen's University Belfast, Grosvenor Road, Belfast, BT12 6BA, UK; d.mcdonald@qub.ac.uk.

where it inhibits intraretinal angiogenesis and increases pathologic intravitreal neovascularization.[7] In the same context, expression of the endothelial isoform of NOS is decreased along with the demise of the endothelium in the vasoobliterative phase and thus precedes the onset of hypoxia. Therefore in this study we sought to investigate if enhancing NO production from eNOS within the endothelium could increase angiogenic drive and accelerate intraretinal vascular recovery.

Analyzing the role of eNOS in disease is complicated by the fact that eNOS, in addition to producing NO, can become dysfunctional or uncoupled and generate the oxygen free radical superoxide (O_2^-) in preference to NO.[19] The consequences of this are 2-fold: first, there is a decrease in bioavailable NO; second, the concomitant increase in O_2^- production leads to elevated levels of peroxynitrite ($ONOO^-$), a highly reactive free radical derived from the reaction of O_2^- with NO. Overall, this process compromises the homeostatic functions of eNOS. Thus eNOS can either be beneficial to vascular health or contribute to disease. This dual role of eNOS in angiogenesis is not well studied. In the retina, free radicals derived from NOS have been shown to trigger apoptotic cell death and capillary closure in response to hyperoxia and diabetes.[13,20–23] This response is believed to be mediated by NOS-derived peroxynitrite. However, the mechanism that leads to enhanced $ONOO^-$ production in hyperoxia is not fully characterized. One possibility is that the increased O_2^- levels derived from enzymes such as NADPH oxidase—upregulated in hyperoxia—reacts with eNOS-derived NO, elevating $ONOO^-$ levels. A second possible pathway is that eNOS acts as a source of O_2^- in addition to producing NO. Mechanistically, this is important to define as therapeutic strategies that address oxidative stress without ensuring correct NOS function could limit the efficacy of such treatments. Moreover, NO has many important vasoprotective functions. Therefore, any disturbance to its function could have detrimental effects for endothelial integrity. There are several possible causes of eNOS dysfunction, including an insufficiency of the essential cofactor, BH_4, or the substrate, arginine. Indeed, there is much evidence to demonstrate that endothelial dysfunction, an early indicator of cardiovascular disease, is caused by an inadequate supply of BH_4 for eNOS to function efficiently.[24] The role of BH_4 in retinal vascular pathology is less well characterized.

The possibility of opposing roles for eNOS in the murine oxygen-induced retinopathy (OIR) model underlines the need to characterize the effect of eNOS overexpression on the hyperoxic and the hypoxic phases.[28] Transgenic animal models with modified eNOS expression have been central to defining the role of eNOS in disease, especially with regard to defining its role in either preventing or exacerbating disease.[25,26] Therefore we used one such strain, an eNOS–green fluorescent protein (GFP) overexpressing model, to further define the role of eNOS in retinal angiogenesis. These animals overexpress eNOS as an eNOS-GFP fusion protein to facilitate identification of the transgenic protein. These animals have been extensively characterized and the presence of the GFP has been shown to have no adverse effect on the activity of the enzyme. In addition, they have similar functional characteristics as eNOS overexpressing animals without the GFP tag, such as a similarly reduced blood pressure, further indicating that addition of GFP has no effect on function.[26–28]

Materials and Methods

Retinal Vascular Parameters: Physiologic Angiogenesis and OIR

Animals overexpressing eNOS-GFP on a C57/BL6 background were used for all experiments. These animals encode the full-length human genomic DNA sequence including the endogenous eNOS promoter, fused in frame with an eGFP reporter sequence allowing expression of an eNOS-GFP fusion protein.[27] Briefly, a genomic DNA fragment including 6 kb of 5′ sequence, the complete eNOS gene, and 3 kb of 3′ sequence was isolated from a human cosmid library. At the STOP codon of the eNOS gene, a linker was introduced that allowed the in-frame insertion of eGFP (derived from the pEGFP-N1 plasmid; Clontech Laboratories, Mountain View, CA). Oocytes from FVB mice were used for microinjections and transplanted into B10×CBA. Offspring were back-crossed to C57Bl6 for at least five generations. Animals homozygous for the transgene are not viable, therefore, heterozygous animals along with their litter mate controls were used throughout and are referred to as eNOS-GFP and wild type (WT). To investigate normal vascular development, eyes were examined at various time points known to be important for vascular development including postnatal (P) days 5, 7, 12, and 17, fixed in 4% paraformaldehyde (PFA) and retinas processed as described in the following text. For OIR treatment, pups on postnatal day 7 (P7) along with their mothers were placed into a high-oxygen (75%) environment for 5 days, resulting in vaso-obliteration of the central retinal vasculature as described previously.[8,29,30] At P12 the mice were returned to room air and euthanized at intervals between P12 and P17. One eye of each animal was fixed in 4% PFA for immunostaining or cyropreserved in optimal cutting temperature (OCT) medium for subsequent cryosectioning; the other retina was snap frozen and stored at −70°C for later protein extraction. All animal studies were performed under a project license issued by the UK Home Office (Animals Scientific Procedures Act 1986), approved by the local animal care ethics committee and conducted in accordance with the ARVO statement for the use of animals in ophthalmic and vision research.

Retinal Flat-Mount Processing and Analysis

Lectin Staining of Vasculature in the Murine Retina. PFA-fixed eyes were flat mounted and blood vessels labeled with biotinylated isolectin as described.[30] Briefly, specimens were treated with permeabilization buffer (PBS with 0.5% Triton-X-100, 1% normal goat serum, 0.1 mM $CaCl_2$, 0.05% NaN_3) for 4 hours at 37°C and incubated with biotinylated GS isolectin B4 (20 μg/mL; Sigma-Aldrich, Dorset, UK) overnight at 4°C followed by strepavidin conjugate (Alexa-Fluor 568; Molecular Probes, Eugene, OR).

Analysis of Lectin-Stained Retinal Flat Mounts. Lectin-stained flat-mounted retinas were imaged using a fluorescent microscope (Nikon Eclipse E400; Nikon Corporation Instruments Co., Tokyo, Japan). Normal vascular development was assessed by imaging vascular network formation in the superficial, intermediate, and deep retinal layers at P5, P7, P12, and P17. In developing retinas, the vascular plexus migration distances were measured in microns from the edge of the optic disk in each quadrant and averaged to obtain a mean value for each retina. For branch point measurement, high-magnification images were collected adjacent to the leading edge of the vascular plexus or in the central retina using an inverted microscope (Nikon TE2000-U). Branching points were counted by marking forks in the vascular tree. In each image the path of the vessels was followed toward the leading edge of the vascular plexus and the number of forks in the vessels were marked and counted. The total number of branching points was divided by the total area of vascular plexus to correct for any size differences between retinas. For quantification of vaso-obliteration, vascular regrowth, and neovascularization, images were taken at P12, P13, and P17 post-OIR. The vascular, neovascular, and avascular areas were demarcated and measured in each quadrant in square microns using microscope imaging software (NIS Elements Microscope Imaging; Nikon Instruments Inc., Melville, NY). Avascular areas were defined as those that displayed no lectin staining; normal vascular areas as those that resembled a classical chicken-wire type network, generally in the peripheral retina; and neovascular areas as brightly fluorescent tuftlike structures generally found at the vascular/avascular interface. These latter features were further confirmed as being

neovascular extraretinal tufts by re-embedding in OCT medium and cryosectioning of flat-mounted retinas following image capture. In contrast to vascular development, following OIR vascular growth proceeds from the periphery of the retina toward the central retina. Therefore, to estimate branch point measurement at P17 post-OIR, a series of high-power images were taken adjacent to the advancing vasculature front and quantification performed as described above.

Vascular Regression Analysis

Vascular remodeling and regression in retinal flatmounts were estimated by double-staining with B4 isolectin and collagen type IV (Collagen IV polyclonal antibody; AbD Serotec, Oxford, UK). Three high-power Z-series images were then collected from each quadrant and the number of regressed vessels per 0.5 mm^2 determined. Regressed vessels were those that displayed only collagen IV staining, indicating the presence of a basement membrane, but lacking endothelial cells, indicated by the absence of lectin staining. Z-series collection was used to verify that vessels designated as regressed were indeed regressed, as opposed to those migrating to form the deeper retinal layers.

Determination of Nitrite Formation by Griess Assay from Whole Retinal Explants

Following dissection individual retinas were placed into freshly prepared warmed Krebs-HEPES buffer (pH 7.4, composition in mM: 99.01 NaCl, 4.69 KCl, 1.87 $CaCl_2$, 1.20 $MgSO_4$, 1.03 K_2HPO_4, 25.0 $NaHCO_3$, 20.0 Na-HEPES, 11.1 glucose). Wash buffer was replaced with fresh Krebs-HEPES buffer and one retina incubated with 1 μM calcium ionophore (Sigma-Aldrich) to stimulate NO production, whereas the contralateral eye was either used to measure basal (unstimulated nitrite levels) or incubated with calcium ionophore in the presence of the NOS inhibitor L-NAME (1 mM) and incubated at 37°C for 14 hours in a tissue-culture incubator. Conditioned media was removed and nitrite levels determined by Griess assay with measurements corrected for total sample weight. Protein was then extracted from the retinal samples and processed for Western blotting to quantify eNOS and nitrotyrosine levels. Moreover, comparison between eNOS and NT immunoreactivity were similar if taken at 0 hours or following the 14-hour incubation and both were unaltered by ionophore stimulation (see Supplementary Material and Supplementary Fig. S1, http://www.iovs.org/lookup/suppl/doi:10.1167/iovs.12-9797/-/DCSupplemental).[31]

NOS Activity Assay

NOS activity was determined by the conversion of radiolabeled arginine to citulline using a NOS activity assay kit as described previously (Cayman Chemical Co., Ann Arbor, MI) with minor modifications.[30] Pooled mouse retinas were homogenized and added to the reaction mixture containing [^{14}C]arginine (0.05 μCi; Amersham Biosciences, Piscataway, NJ) and incubated 1 hour at 37°C. For comparisons in the presence or absence of additional BH_4, 1 aliquot of retinal lysate was added to a buffer containing BH_4 (3 μM) and another aliquot from the same pool added to a buffer without additional BH_4. A third sample was used for Western blotting to determine NOS isoform expression. Following the 1-hour incubation, ice-cold HEPES buffer containing EDTA (pH5.5) was added and unreacted arginine and ornithine removed by filtration through a spin column before determination of [^{14}C]-L-citrulline levels. For each sample, background was determined by incubation in the presence of L-NNA and subtracted from the total counts. To ensure measurements of NOS activity only the arginase inhibitor (S)-(2-boronoethyl)-L-cysteine-HCl (BEC; 5 μM; Calbiochem/EMD Chemicals, Gibbstown, NJ) was added to all reactions. For NOS activity, $n = 5$ to 6 retinas were pooled and assayed in triplicate.

Aortic Ring Assay

Adult eNOS-GFP and age- and sex-matched WT littermate animals were used for the aortic ring assay and adapted from a protocol for rat aortas.[32] Briefly, following euthanasia the aorta along with the heart was removed and placed immediately in ice-cold DMEM. Following removal of adipose tissue 1-mm rings were cut and placed in 96-well plates precoated with prepolymerized gelatinous protein mixture (Matrigel; BD Biosciences, Franklin Lakes, NJ)/PBS mixture (1:1) and embedded in additional protein (Matrigel/PBS) mixture (1:1). Following polymerization, DMEM containing 10% fetal calf serum (Gibco/Invitrogen Ltd., Paisley, UK) with or without 1 mM NG-nitro-L-arginine methyl ester (L-NAME) was added to each well. The medium was changed every 2 days and specimens fixed after 7 days. Following image capture the numbers of branch points at the perimeter of the aortic ring were quantified. Vessel density was quantified using microscope imaging software (NIS Elements). Endothelial cell identity in explants was confirmed by PECAM and anti-GFP immunolabeling with FITC conjugated anti-GFP (Abcam) or PECAM.

Detection of Reactive Oxygen and Nitrogen Species

Sample Preparation. Freshly isolated whole eyes were embedded in OCT compound (Tissue-Tek; Fisher Scientific, Waltham, MA) using liquid nitrogen cooled isopentane and eyes vertically sectioned at 10 μm, mounted on slides (Superfrost Plus; Menzel-Gläser, Braunschweig, Germany) and stored at −20°C until use.

Dihydroethidium (DHE) as an In Situ Fluorescent Indicator of Superoxide Production. In situ superoxide production was quantified with the oxidative fluorescent dye dihydroethidium (DHE) as previously described.[30] Briefly, serial cryosections (10 μm) were preincubated for 30 minutes at room temperature in PBS in the presence or absence of each of the following inhibitors: polyethylene glycol-superoxide dismutase (PEG-SOD, 400 U/mL), or L-NAME (1 mM). Sections were then incubated with DHE (10 μM) in the presence or absence of the same inhibitors for 1 hour at 37°C in a dark humidified chamber. DHE images were obtained using a confocal laser-scanning microscope (CLSM 2000; Bio-Rad Micro-Radiance; Bio-Rad, Hercules, CA) at a magnification of ×400 and identical acquisition settings maintained for collection of all images. For P12 analysis, the ganglion cell layer (GCL), where the vessels reside (or pre-OIR, had been located), was demarcated (see Supplementary Material and Supplementary Fig. S9, http://www.iovs.org/lookup/suppl/doi:10.1167/iovs.12-9797/-/DCSupplemental). For the P17 post-OIR sections, NV tufts were demarcated and fluorescence corresponding to these quantified by automated image analysis using ImageJ software (developed by Wayne Rasband, National Institutes of Health, Bethesda, MD; available at http://rsbweb.nih.gov/ij/index.html). For each treatment a mean fluorescence value was determined from 8 images (from at least 6 sections) per eye and three eyes were assayed per experimental group from three independent OIR experiments.

Nitrotyrosine Immunolocalization in Retinal Sections. Nitrotyrosine (NT) is the stable end product of reactions between peroxynitrite and tyrosine residues on cellular proteins; it is therefore a useful surrogate marker of peroxynitrite. Freshly cut retinal sections were fixed with 4% PFA for 30 minutes at room temperature. Sections were permeabilized using PBS with 0.3% Triton-X-100. Tissue was blocked with 5% NGS containing 0.1% Triton-X-100 in PBS for 30 minutes followed by 30 minutes in 1% BSA in PBS prior to antigen detection with polyclonal antinitrotyrosine antibody (06-284; Upstate/Millipore, Billerica, MA) and secondary antibody (Alexa-Fluor 568).

Measurements of nitrotyrosine staining intensity were made using Image J software. The neovascular tuft areas, graded as nuclei reaching above the retinal surface, in P17 specimens were demarcated in the images using the DAPI staining as a guide. For P12 data, the GCL was demarcated and fluorescence in this layer quantified. For each group a mean fluorescence value was determined from at least 10 images per

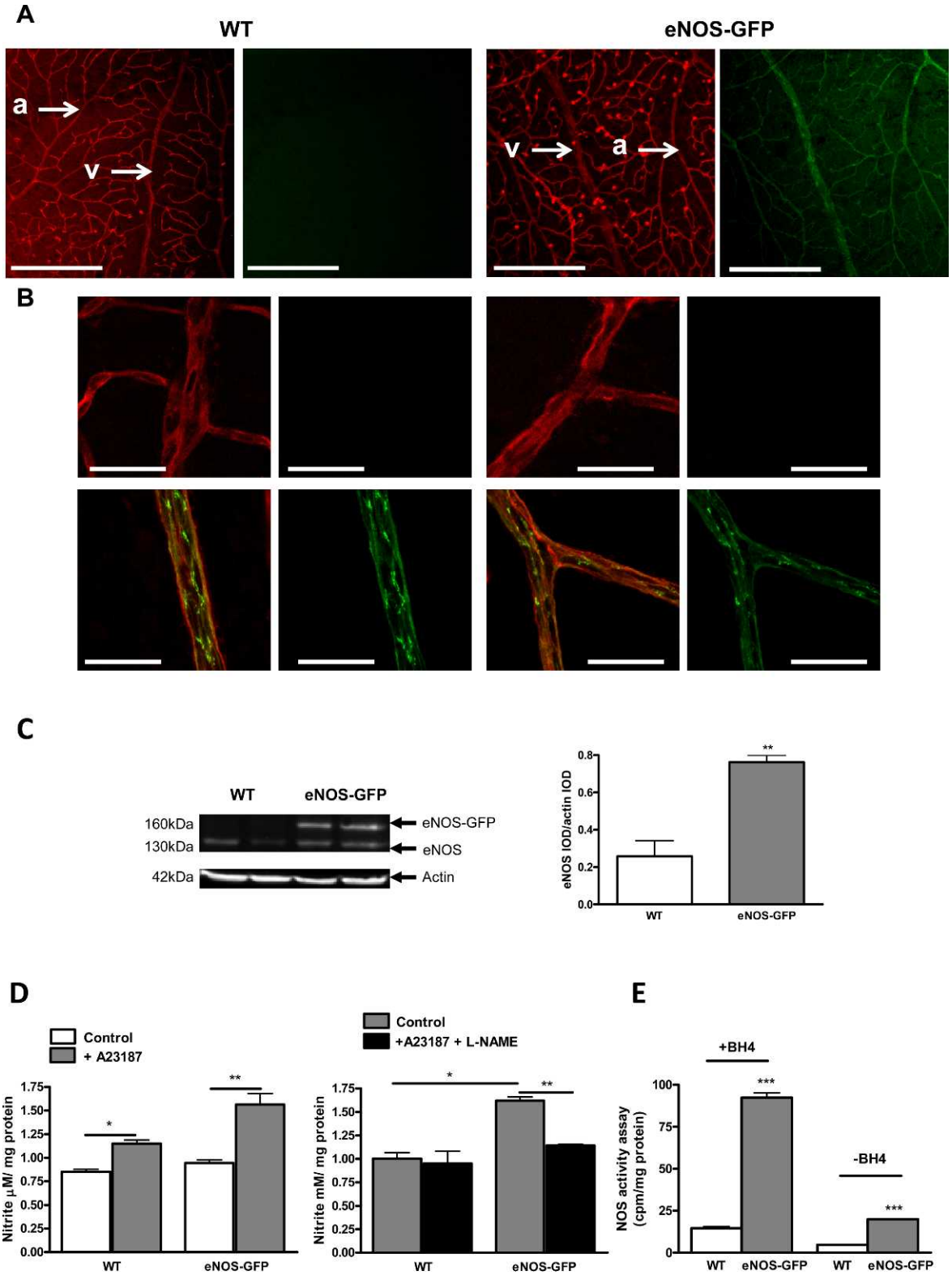

Figure 1. Characterization of eNOS-GFP transgene expression in the retinas of adult mice. (**A**) Visualization of retinal vessels with lectin (*red*) shows uniformity of eNOS-GFP expression throughout the retinal vascular tree and specific EC localization of eNOS (*green*). Examples of an arteriole and vein (*arrows*) are highlighted in each image. (**B**) Higher-magnification image demonstrates the typical plasma membrane and Golgi localization of eNOS. (**C**) Western blotting of retinal lysates confirms the presence of eNOS-GFP fusion protein expression (160 kDa) and endogenous murine eNOS (130 kDa); examples of two individual retinas are shown for each genotype. (**D**) Nitrite production was measured using a Griess assay on isolated whole retinas from adult eNOS-GFP and WT mice in the presence or absence of A23187 and L-NAME ($n = 2$–3 independent experiments each performed on three eyes). (**E**) NOS activity assay measured as the conversion of radiolabeled arginine to citrulline in the presence or absence of BH_4 ($n = 5$ retinas/group). $^*P < 0.05$, $^{**}P < 0.01$, $^{***}P < 0.001$. Arterioles (a) and veins (v). *Scale bars*: (**A**) 500 µm; (**B**) 50 µm.

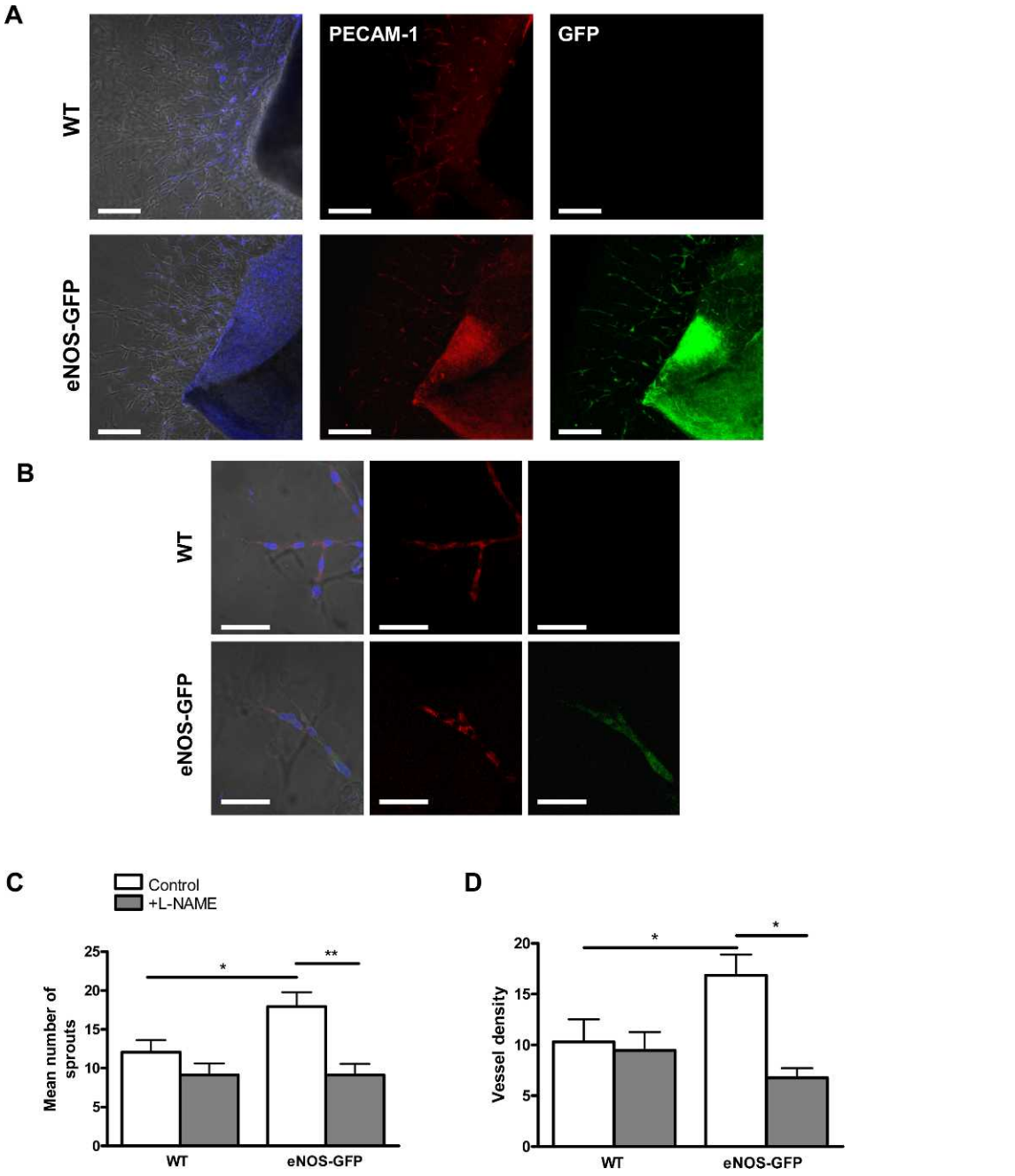

Figure 2. Tube formation in aortic explants from eNOS-GFP mice compared with WT. Aortic rings were embedded in a gelatinous protein mixture (Matrigel) and cultured for 7 days in DMEM with 10% FCS with and without L-NAME. (**A**, **B**) Aortic rings stained with PECAM-1 (*red*) and counterstained with DAPI nuclear stain (*blue*) demonstrate colocalization with endothelial eNOS-GFP. Higher-power images in (**B**). (**C**) Quantification of branching and (**D**) vessel density in the presence and absence of L-NAME. $^{*}P < 0.05$, $^{**}P < 0.01$; $n = 4$ to 6 aortic rings per group in 7 to 8 independent experiments. *Scale bars*: (**A**) 500 μm; (**B**) 100 μm.

eye to give $n = 1$, three eyes were assayed per experimental group from three independent OIR experiments.

Western Blotting

Retinas were thawed on ice and prepared as described previously.[30] Equivalent amounts of protein sample, typically 30 μg, were separated on a 9% SDS-polyacrylamide gel and proteins transferred to polyvinylidene difluoride membrane (Pall Corporation/Life Sciences Division, Port Washington, NY) and immunostained with anti-eNOS (BD Biosciences), monoclonal anti-nitrotyrosine (Cayman Chemical Co.) primary antibodies, followed by the appropriate horseradish peroxidase (HRP) conjugated secondary antibody (Santa Cruz Biotechnology, Santa Cruz, CA). To verify equivalency of loading, the membrane was probed with β-actin mouse monoclonal antibody (Sigma-Aldrich). The membrane-bound protein was detected by enhanced chemiluminescence (Immobilon Western chemiluminescent HRP substrate; Millipore Corp.) in accordance with the manufacturer's instructions. Images were acquired using a commercial imaging system (AutoChemi Imaging System; UVP BioImaging Systems, Upland, CA). Band densitometry was performed on images using imaging system software (Labworks v4.08; UVP BioImaging Systems). Quantification of

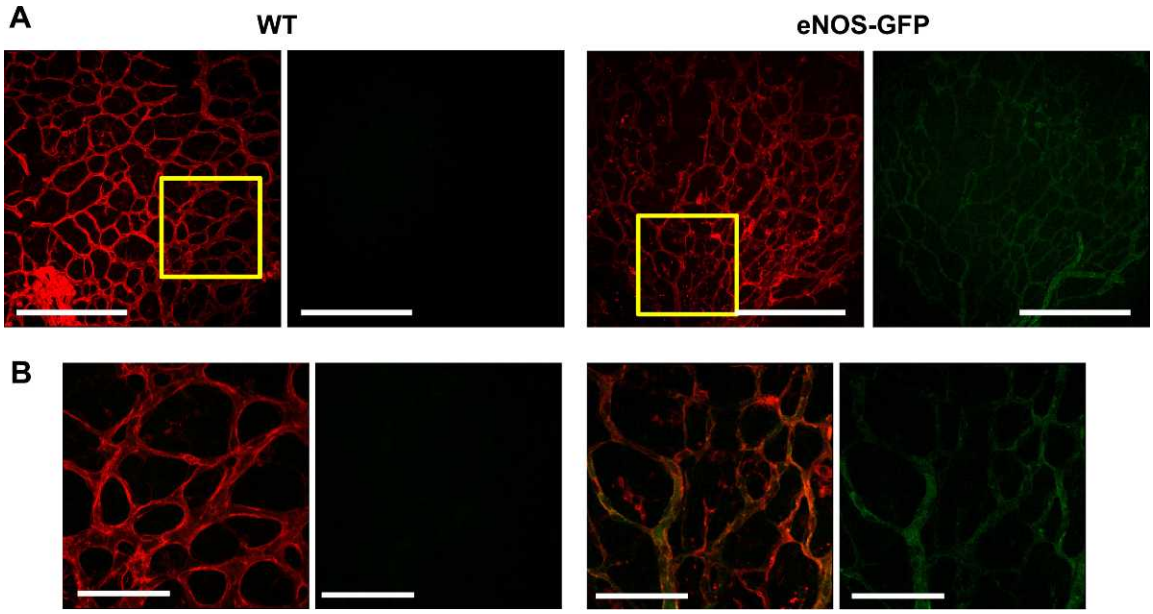

Figure 3. eNOS-GFP expression in developing retinal vessels of the inner retina at P5. (**A**) GFP fluorescence is clearly visible in the developing vasculature and colocalizes with lectin-stained vessels. Representative images of retinal flat mounts stained with lectin. (**B**) High-magnification images of those sections highlighted in the *yellow boxes* in (**A**). *Scale bars*: (**A**) 500 μm; (**B**) 100 μm.

eNOS in Western blots refers to total eNOS expression (eNOS + eNOS-GFP) unless otherwise stated.

VEGF ELISA

Individual retinas at P13 or P17 post-OIR were homogenized in 150 μL of PBS in the presence of protease inhibitors. After two freeze–thaw cycles were performed to break the cell membranes, the homogenates were centrifuged for 5 minutes at 5000*g* and VEGF in the supernatant was determined by ELISA (R&D Systems, Minneapolis, MN) following the manufacturer's instructions. Values were expressed relative to the protein content of the sample.

Statistical Analysis

Statistical analysis was performed by independent Student's *t*-test to determine differences between groups ($^{*}P < 0.05$; $^{**}P < 0.01$; $^{***}P < 0.001$). When comparisons between more than two groups were performed, ANOVA was used to determine statistical significance followed by Tukey's post hoc testing. All data are presented as ± SEM from 3 to 6 individual OIR experiments unless otherwise indicated.

Results

Retinal Expression of eNOS-GFP in Adult Animals

eNOS-GFP expression in retinal vessels of adult animals showed restricted expression to the endothelium along with the typical subcellular localization to the plasma membrane in endothelial cells (Fig. 1). In addition, GFP fluorescence was absent in other retinal cell types. Calcium ionophore produced a measurable increase in nitrite production, which was inhibitable with L-NAME, confirming NOS-dependent nitrite generation (Fig. 1D). Functionality of the eNOS-GFP fusion protein was shown by a 1.6-fold increase in nitrite formation comparable to the increase in eNOS protein (3-fold) in these animals (Figs. 1C, 1D). NOS activity assay in the presence of additional BH_4 showed a 4-fold increase in eNOS activity compared with WT controls, which was similar to the difference in eNOS expression between the groups. In the absence of BH_4, although total NOS activity was reduced overall, there was still a comparable and significant difference in eNOS activity between the groups, indicating a correlation between protein levels and activity (Fig. 1E).

Effect of eNOS Overexpression on Branch Formation and Vascular Coverage in Aortic Explants

The aortic ring assay was used as an accessible in vitro system to investigate the effect of eNOS overexpression on angiogenic processes in vitro. When aortic rings from WT and eNOS-GFP mice were embedded in gelatinous protein mixture (Matrigel), there were significantly more sprouts formed in explants from eNOS-GFP mice (Fig. 2). Addition of L-NAME decreased sprout formation in both groups with a significant difference seen in the eNOS-GFP animals with the number of sprouts falling from 18.9 ± 1.8 to 9.3 ± 1.7 with L-NAME. In agreement with this, quantification of vascular density also showed significantly more profuse branching of the network of tubes in eNOS-GFP explants. Again the density of branching was reduced upon addition of L-NAME.

Effect of eNOS Overexpression on Physiologic Vascular Development

Normal vascular development in all animals was determined by analysis of network formation at P5, P7, P12, and P17, which showed comparable degrees of vascularization in each of the retinal layers, a superficial layer at P5, and formation of the deeper layers from P7 through to P12 and P17 including similar evidence of arterial and venous specification in both groups (see Supplementary Material and Supplementary Figs. S2, S3, http://www.iovs.org/lookup/suppl/doi:10.1167/iovs.12-9797/-/DCSupplemental). GFP expression coincided with lectin positive vessel staining at each of the time points examined, P5, P7, P12, and P17 (Fig. 3 and Supplemental Fig. S4 [see Supplementary Material and Supplementary Fig. S4, http://www.iovs.org/lookup/suppl/doi:10.1167/iovs.12-9797/-/DCSupplemental]),

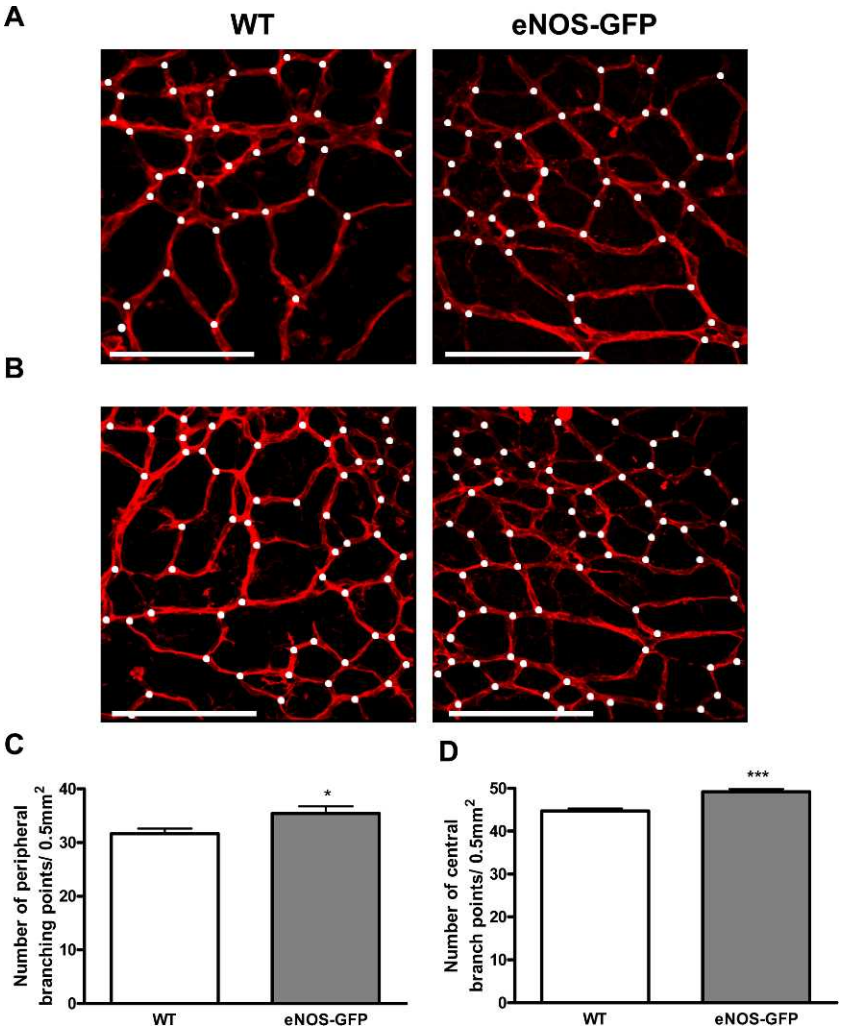

Figure 4. The effect of eNOS overexpression on vascular density in the developing retina at P7. Representative images of vascular branching in WT and eNOS-GFP retinal flat mounts stained with lectin taken from the (**A**) peripheral and (**B**) central retina. Branching points are marked with *white dots*. (**C**, **D**) High-magnification images were captured adjacent to the leading edge of the vascular plexus and in the central region to estimate vascular branching. $^{*}P < 0.05$, $^{***}P < 0.001$; $n = 8$ WT, 10 eNOS-GFP. *Scale bars*: (**A**) 100 μm.

confirming transgene expression at early stages of inner retinal vascular development and demonstrating that the regulatory elements in the human promoter recapitulate those present in the murine promoter. Furthermore, analysis of vascular development at P7 demonstrated that there was no significant difference in the maximum vascular plexus migration distances, as measured from the optic disc to the retinal periphery, in the developing retina of eNOS-GFP mice compared with WT littermates. There was, however, a small but statistically significant increase in the density of the vascular plexus and in branch formation in the eNOS-GFP group (Fig. 4). This difference was also evident at P5 and P17 in room air control animals (see Supplementary Material and Supplementary Figs. S5, S7, http://www.iovs.org/lookup/suppl/doi:10.1167/iovs.12-9797/-/DCSupplemental).

To further investigate if the increased vascular density seen in the primary vascular plexus at P7 was due to changes in vascular remodeling or pruning between the genotypes we performed collagen IV staining of retinal flatmounts at P7 (Fig. 5). Following vessel remodeling the basement membrane protein collagen IV is preserved, which results in the appearance of collagen IV positive, lectin negative vessels. There was no significant difference in the number of pruned vessels in the vasculature of WT retinas and eNOS-GFP retinas. This was also the case for retinas taken from room air control animals at P5 and P17 (see Supplementary Material and Supplementary Figs. S6, S8, http://www.iovs.org/lookup/suppl/doi:10.1167/iovs.12-9797/-/DCSupplemental). Analysis of deep plexus formation during normal retinal development (P5/P7) also demonstrated normal development of the deep and intermediate retinal vascular plexuses in both groups (see Supplementary Material and Supplementary Fig. S3, http://www.iovs.org/lookup/suppl/doi:10.1167/iovs.12-9797/-/DCSupplemental).

Effect of Hyperoxia-Induced Vaso-Obliteration on eNOS Overexpression

Vaso-obliteration in WT and eNOS-GFP mice was estimated at P12 following 5 days of hyperoxia. There was a significant increase in the avascular area in eNOS-GFP transgenic mice, indicating increased severity of vaso-obliteration (Fig. 6). At the same time point, NOS protein levels were 2-fold higher in the eNOS-GFP group despite evidence of less vasculature posthyperoxia, suggesting more eNOS-GFP protein expressed/cell (Fig. 7). This difference in expression was also reflected in the enhanced NOS activity in this group. Importantly, this obvious difference was lost when additional BH_4 was not supplied, indicating that the

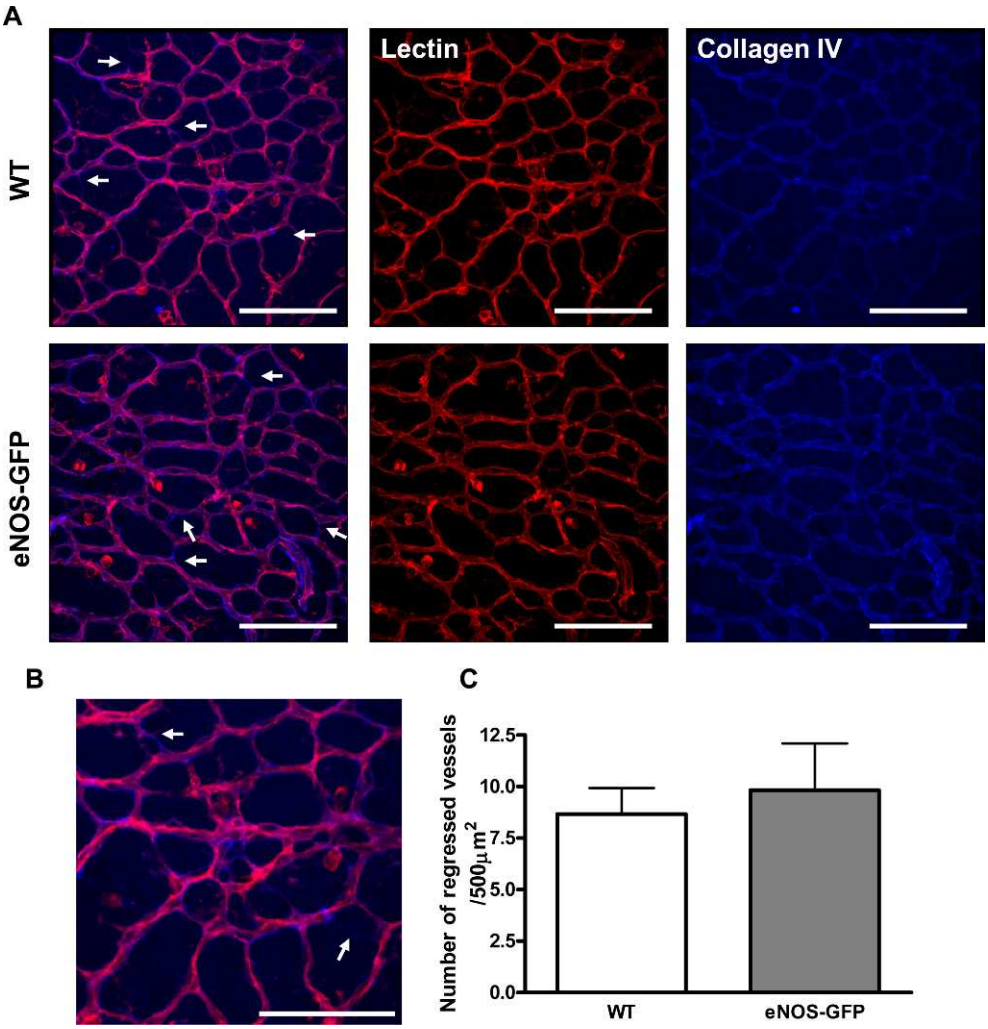

Figure 5. Vessel regression in developing P7 retinal vasculature. Flat-mounted retinas from WT and eNOS-GFP mice were stained with lectin and collagen IV to investigate vessel remodeling. Remodeled vessels were those that are collagen IV positive and lectin negative (*arrows*). (**B**) An enlarged area of the image from (**A**). (**C**) Quantification of collagen IV positive, lectin negative vessel fragments ($n = 5$–8 per group). *Scale bars*: 100 μm.

endogenous BH_4 levels in the sample were not sufficient to meet the demands of the additional eNOS. This decreased NO production from eNOS in hyperoxia suggested that eNOS may be uncoupled and producing superoxide in addition to NO. Indeed, this was further substantiated by demonstration of enhanced vessel-associated DHE florescence in the eNOS-GFP group post-OIR, which, importantly, was inhibited by L-NAME, providing further evidence that eNOS was the source of this superoxide. This also correlated to enhanced NT immunofluorescence in the same layer. NT is a long-lasting marker of $ONOO^-$ activity and accordingly was also found to be elevated in the GCL of the avascular retina at P12 posthyperoxia (see Supplementary Material and Supplementary Fig. S9, http://www.iovs.org/lookup/suppl/doi:10.1167/iovs.12-9797/-/DCSupplemental).

Vascular Regrowth following OIR: Revascularization versus Pathologic Neovascularization

Following hyperoxia exposure, when mice are returned to room air the ensuing hypoxia in the central retina induces neovascularization. We investigated the vasculature of WT and eNOS-GFP mice at P13 in retinal flat mounts stained with lectin. There was no immediate regrowth of vasculature following return of the animals to room air in WT animals and a negligible increase in vascular area seen in eNOS-GFP animals (data not shown). Because of the increased vaso-obliteration in these animals it was important to express the values for vascular growth by P17 relative to P12. Total vascular growth by P17 relative to P12, was significantly greater in eNOS-GFP mice compared with WT (Fig. 8), resulting in equivalent amounts of avascular area between the two groups. Further characterization of the vascular phenotype showed that it consisted of increased normal vasculature in addition to NV tuft formation (Fig. 9). Estimation of branching at the interface between the avascular/vascular interface showed that the density of vascular branching was significantly increased in eNOS-GFP animals relative to WT (Fig. 10).

Nitrite Production and NOS Activity in P17 Post-OIR Retinas

NOS activity in eNOS-GFP and WT retinal extracts at P17 post-OIR was compared with age-matched retinas not subjected to OIR (room air control: RAC). In the RAC group there was a 2-fold increase in activity in the eNOS-GFP group irrespective of the presence of additional BH_4. This 2-fold difference in activity

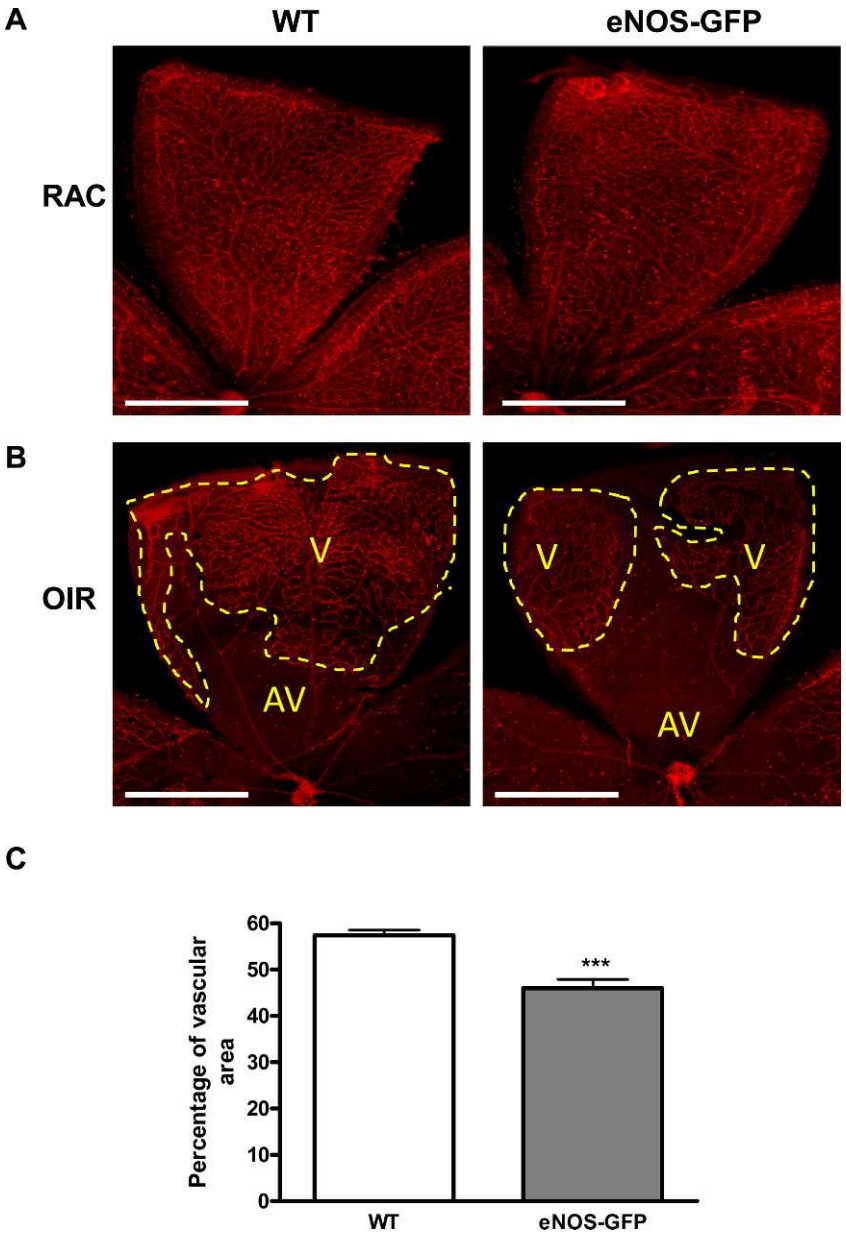

Figure 6. Quantification of vascular closure following hyperoxia at P12. Neonatal animals at P7 were exposed to high oxygen for 5 days to induce vaso-obliteration in the central retina. Retinal flat mounts were prepared and the remaining vascular bed was stained with lectin and quantified. Representative images from WT, eNOS-GFP. (**A**) Flat mounts of room air control animals (RAC) at P12 and (**B**) following OIR showing vascular (V) and avascular (AV) areas. (**C**) The percentage vascular area was determined by measuring vascular areas (V) and total retinal area. There was a significantly greater avascular area in eNOS-GFP retinal flat mounts compared with WT. $^{***}P < 0.001$. *Scale bar*: (**A**) 500 μm.

reflected the 2-fold increase observed in protein expression demonstrated by Western blotting. In contrast, in the OIR-treated group, despite a 10-fold increase in total eNOS expression compared with WT, this translated into only a moderate increase in NO activity. Significantly, in the absence of BH_4, this difference was completely lost. NO production was also measured using a Griess assay on intact freshly isolated retinas following OIR and also showed a marginal although still significant increase (1.6-fold) in nitrite production from eNOS-GFP retinas compared with WT when corrected for total protein or retinal weight. This disparity between protein expression and NO production suggests that NOS function was compromised and producing superoxide as well as NO. This was confirmed further by a 2.4-fold increase in NT levels (Fig. 11). Importantly, there was also no significant change in iNOS or nNOS protein levels found in retinal samples from WT and eNOS-GFP mice at P17 (see Supplementary Material and Supplementary Fig. S10, http://www.iovs.org/lookup/suppl/doi:10.1167/iovs.12-9797/-/DCSupplemental).

Investigation of Reactive Oxygen and Nitrogen Species in NV Tufts Post-OIR

Quantification of Nitrotyrosine. NT immunofluorescence in the neovascular tufts in sections from P17 OIR retinas from WT and eNOS-GFP mice was significantly greater in retinas from eNOS-GFP mice (Fig. 12A) and colocalized to eNOS expressing neovascular tuft regions.

Quantification of Superoxide Production Using DHE. We investigated in situ superoxide formation in retinal sections

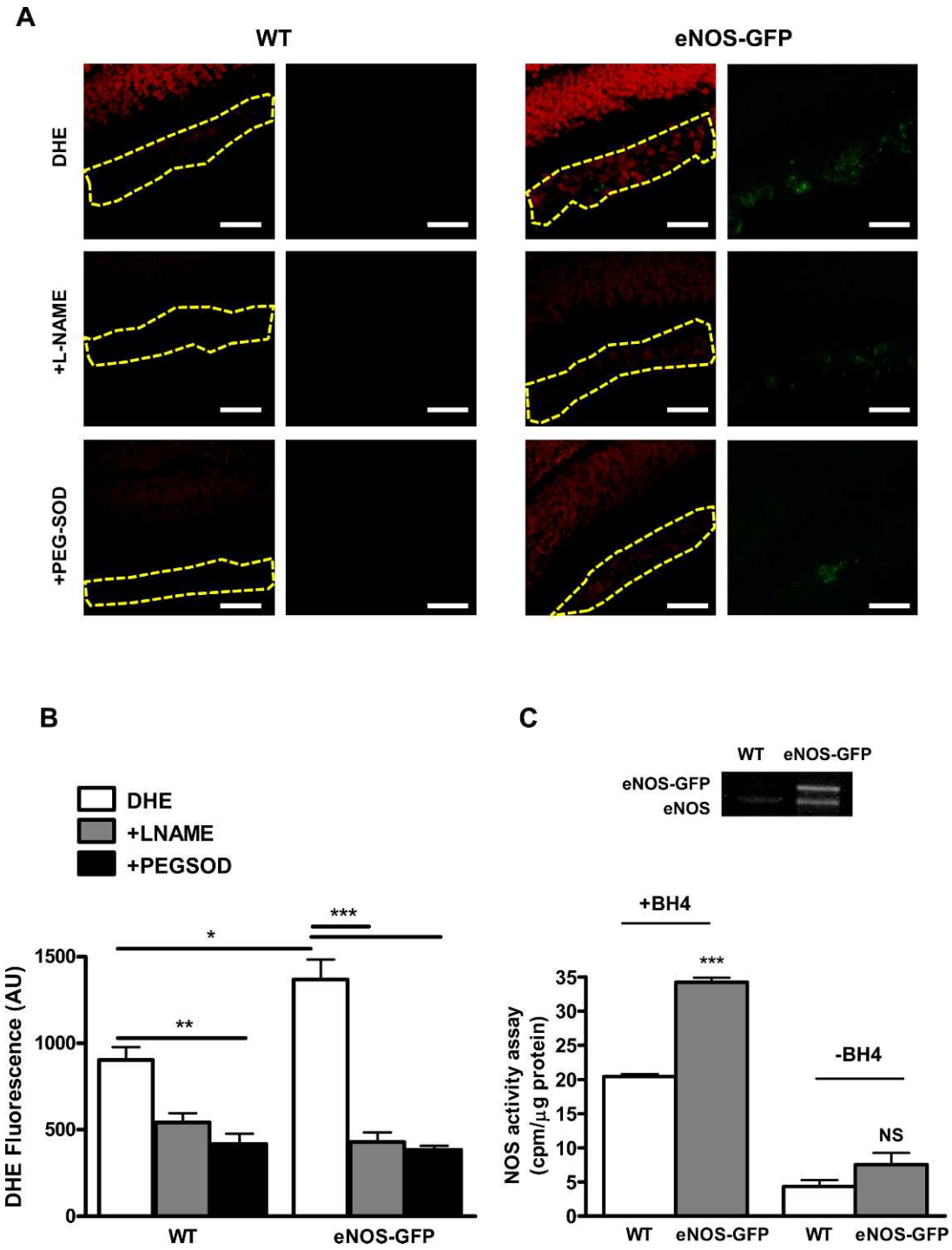

Figure 7. Quantification of superoxide and nitric oxide production in the retina at P12 post-OIR. (**A**) O_2^- generation was assessed using the oxidative fluorescent dye DHE in cryosections in the presence or absence of PEG-SOD or L-NAME. Representative image of DHE (*red*) staining intensity in the vessel containing GCL demarcated with the *yellow outline*. In the eNOS-GFP group there was a marked increase in *red* fluorescence intensity, indicating an increase in the levels of O_2^- formed. Inhibition by L-NAME indicates NOS as a source of O_2^-. (**B**) Quantification of DHE staining shown in (**A**). $n = 3$ from different OIR experiments. *Scale bars*: 50 μm. (**C**) NOS activity assay arginine–citrulline conversion in the presence or absence of BH_4; $n = 5$ retinas/group. Western blotting shows eNOS and eNOS-GFP expression in corresponding retinal lysates. $^*P < 0.05$, $^{**}P < 0.01$, $^{***}P < 0.001$.

from P17 mice specifically in neovascular tuft regions using the oxidative fluorescent dye DHE (Fig. 12C). DHE fluorescence, which was inhibitable with PEG-SOD and L-NAME, was significantly increased in the neovascular tufts in eNOS-GFP animals compared with WT, suggesting eNOS as a possible source of superoxide production.

VEGF ELISA

VEGF expression is increased in line with hypoxia and is induced between P12 and P13 in response to tissue hypoxia. To investigate the possibility that the enhanced growth drive between P12 and P17 may be due to the exacerbated vascular

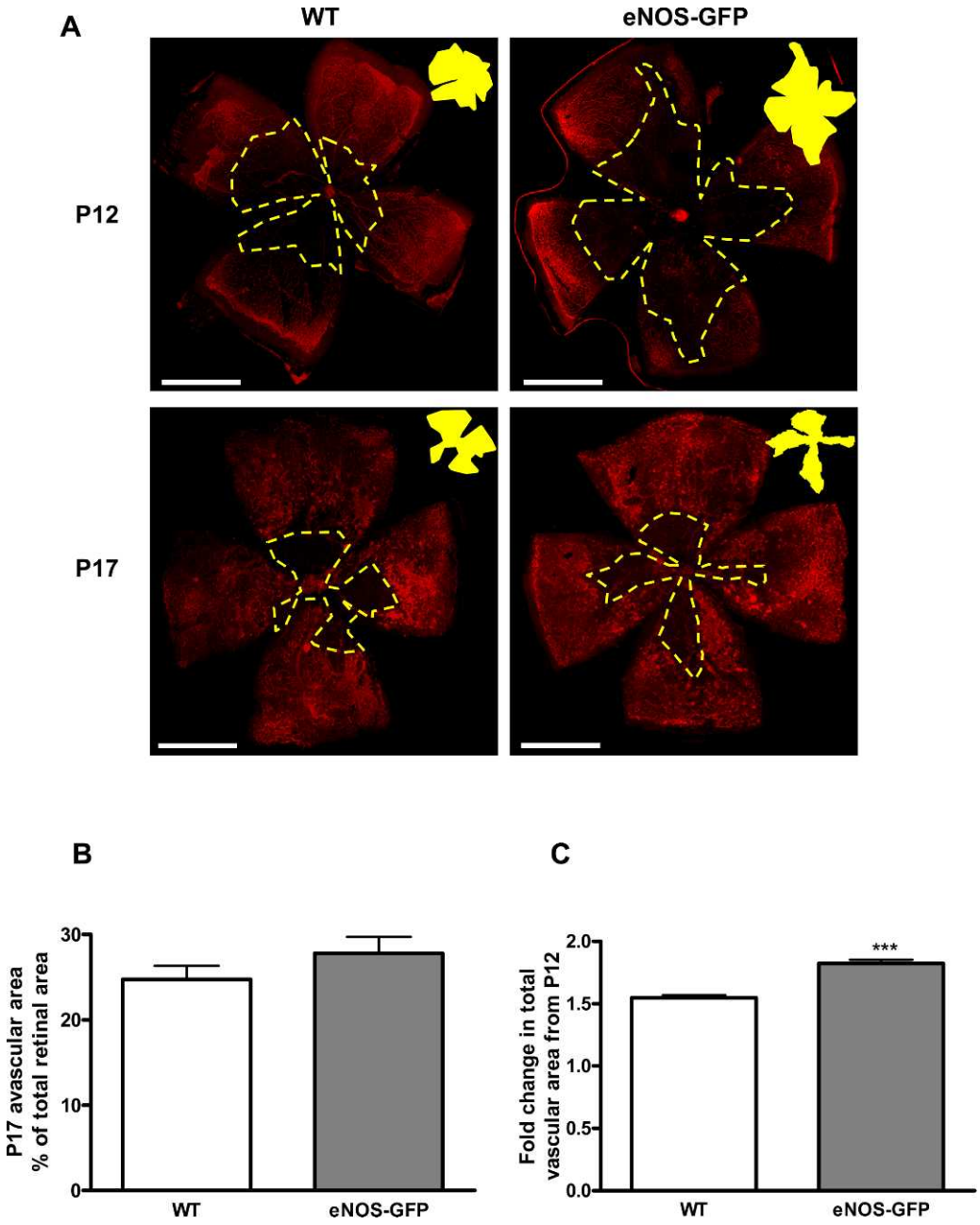

Figure 8. Increased angiogenic growth in eNOS-GFP mice following OIR: change in total vascular area from P12 to P17. There is greater total vascular growth from P12 to P17 in eNOS-GFP animals compared with WT. (**A**) Lectin-stained retinal flat mounts taken at P12 and P17 showing the central ischemic region (*yellow area*). Eyes were collected from animals after 5 days exposure to 75% O_2 causing vaso-obliteration in the central retina. Retinal flat mounts were prepared and stained with lectin to show vasculature. (**B**) The percentage avascular area at P17 and (**C**) the extent of vascular regrowth. $^{***}P < 0.001$. *Scale bars*: (**A**) 500 μm.

closure at P12, we measured VEGF levels at P13 (acute hypoxic phase) and P17 as a measure of hypoxic drive. Importantly, VEGF levels were comparatively lower in the eNOS-GFP group at P13, suggesting the enhanced angiogenic drive in these retinas was indeed eNOS driven (Fig. 13). By P17, the expression of VEGF reached that found in the WT group.

Discussion

Therapeutic strategies that would redirect new vessel growth into the ischemic retina and away from the vitreous would be extremely beneficial for patients with proliferative retinopathy. Here, our aim was to investigate the consequences of eNOS overexpression on vascular closure and to determine if supplemental eNOS could accelerate vascular recovery in the ischemic retina.[9,10,13] To do this we used a well-characterized transgenic strain of eNOS-GFP overexpressing animals previously shown to increase eNOS activity in other models of disease.[27] Initially, we characterized expression of eNOS-GFP in retinas from adult mice. The eNOS-GFP transgene was restricted to an endothelial localization in the retina as demonstrated in retinal flat mounts. In addition, the typical plasma membrane localization of the eNOS-GFP also confirmed that the important posttranslational modifications necessary for subcellular targeting and receptor-mediated activation were

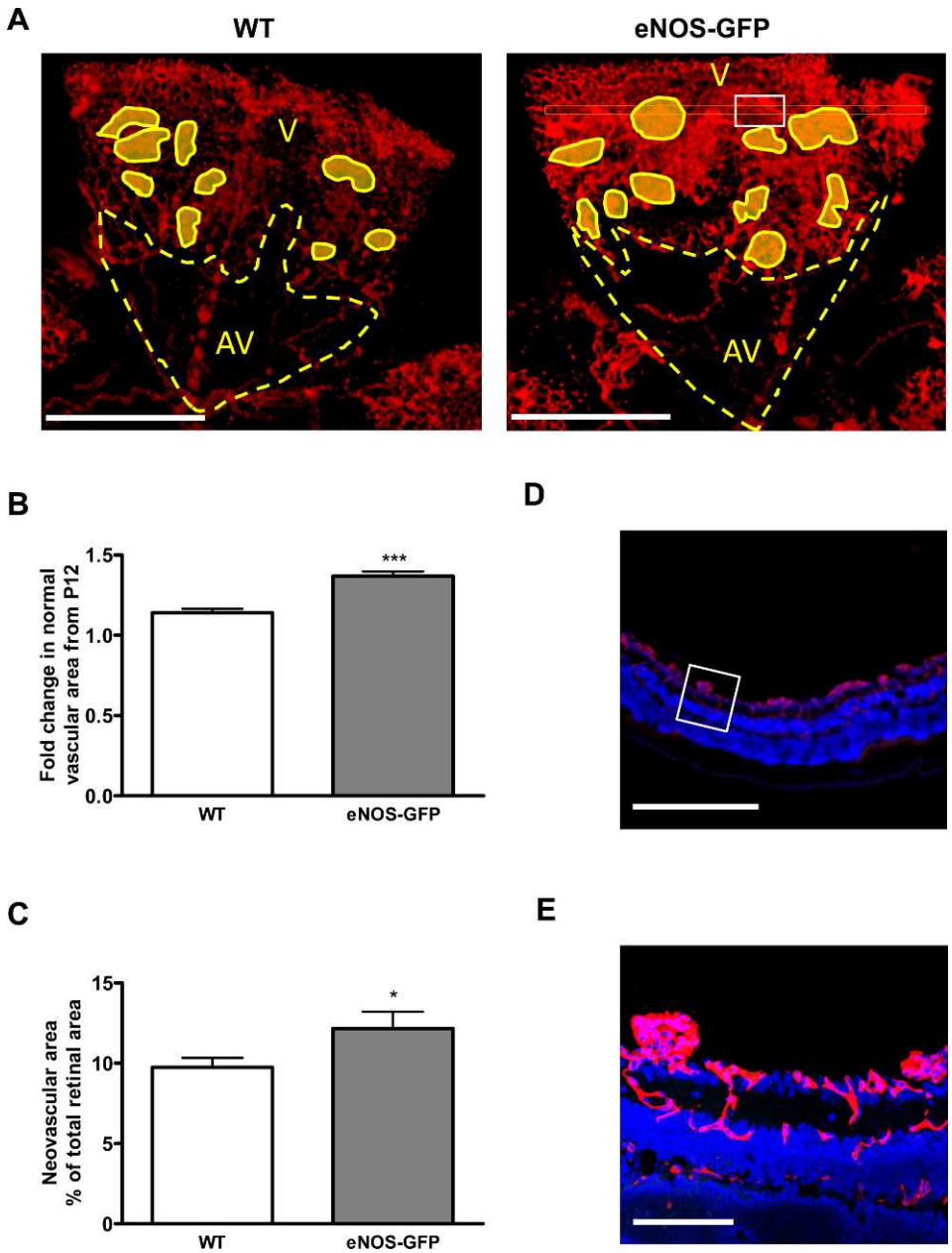

Figure 9. Pathologic neovascularization versus revascularization in P17 eNOS-GFP mice. (**A**) Representative images from retinal flat mounts of WT and eNOS-GFP mice at P17 stained with lectin to show the vasculature. Normal vascular (V), avascular (AV), and neovascular (*shaded areas*) areas were demarcated and measured using image-analysis software. (**B**) Fold change in normal vascular growth from P12 to P17. (**C**) Estimation of neovascular area. (**D**, **E**) Confirmation of extraretinal neovascular tufts in flat-mounted retinas. Lectin-stained retinal flat mounts were sectioned to show that areas designated as neovascular were extraretinal. (**A**) shows flat-mount image before sectioning. (**D**) A section taken from the area indicated by the *white rectangle* in (**A**) (*right panel*). (**E**) A high-power magnification of the *white square* in (**D**). *Scale bars*: (**D**) 500 μm; (**E**) 100 μm. $^{*}P < 0.05$, $^{***}P < 0.001$.

unaffected by the presence of the GFP in accordance with previous studies.[33–38] Western blotting revealed a 3-fold increase in eNOS protein expression in the adult eNOS-GFP mice compared with the WT littermates, which correlated to a 1.6-fold increase in nitrite production, confirming functionality of the protein. Furthermore, NOS activity assay revealed a similar fold increase in enzymatic activity even in the absence of additional BH_4, which correlated closely to the level of eNOS expression. This suggests that BH_4 bioavailability was adequate to supply the demands of the additional eNOS in the adult retina.

eNOS-deficient mice have impaired angiogenesis and wound healing and, conversely, increased expression and activity of eNOS promotes angiogenic drive, increases vessel density, and improves wound healing.[13–16,40–42] Thus having demonstrated functional overexpression of eNOS in the eNOS-GFP animals, we wanted to investigate any role such overexpression may have on vascular development in these mice. Murine retinal vascular development occurs postnatally between day 0 and day 17 and develops radially from the optic disk, driven by VEGF in response to physiologic hypoxia in the inner retina.[39] Thus we initially confirmed vessel-associated transgene expression in P5 retinas and that development of all

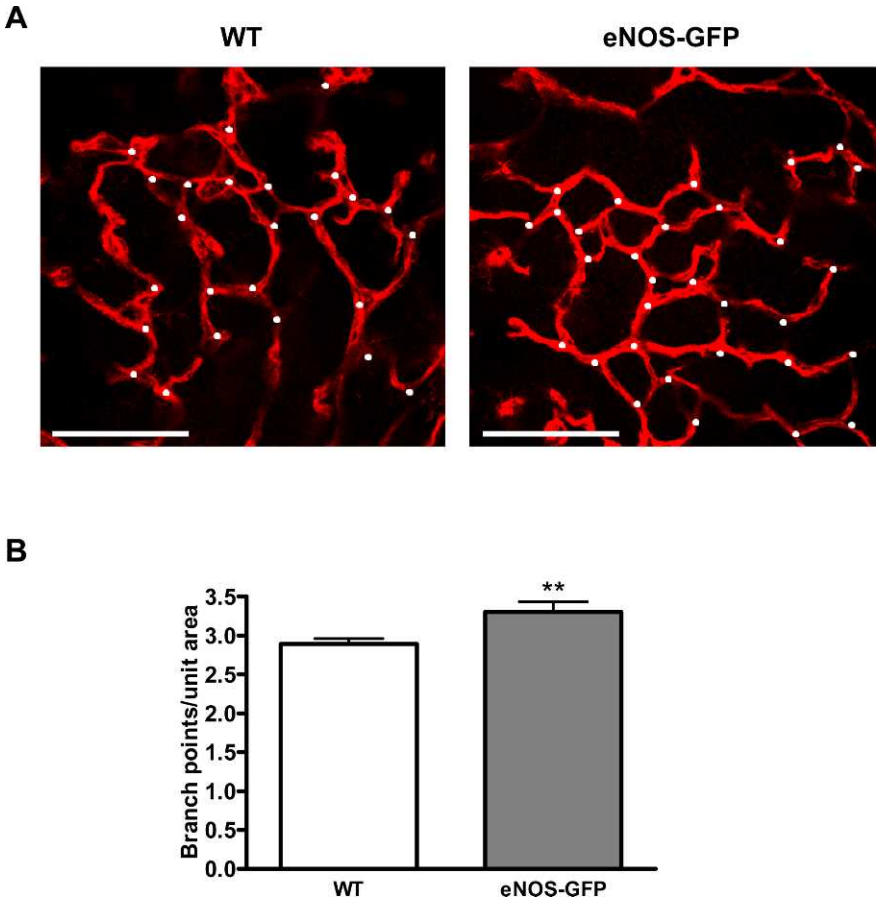

Figure 10. The effect of eNOS overexpression on branching at P17 post-OIR. Retinal flat mounts stained with lectin. (**A**) Representative images of branching in WT and eNOS-GFP retinal flat mounts; branching points are marked with *white dots*. (**B**) High-power images were captured adjacent to the leading edge of the vascular plexus as it revascularizes toward the ischemic central retina. $^{**}P < 0.01$. *Scale bars*: 100 μm.

vascular layers was normal. We also investigated the extent of vascular coverage at P5, P7, and P17 and showed that there was an increase in vascular branching in the eNOS group consistent with a role for NO in stimulating branching during angiogenesis.[40–42]

Next, to determine if the increased vessel complexity was due to decreased vascular remodeling or increased angiogenic drive, we estimated the level of capillary pruning by collagen IV staining, which showed no difference between WT and eNOS-GFP at any of the time points measured (P5, P7, and P17). This indicates that the increase in vessel density noted in the eNOS-GFP animals is due to an increase in angiogenesis and not to a decrease in physiologic pruning. Our in vitro experiments using the aortic ring assay also showed that there was increased angiogenesis in samples from eNOS-GFP mice. There was a significant increase in the number of tubes formed and also increased branching of the tube network in explants from eNOS-GFP animals that could be reduced by addition of L-NAME, suggesting the increased angiogenic potential was inherent to the endothelial cells (ECs).

Following on from the discovery that there is augmented angiogenesis in the eNOS-GFP mice both in vitro and in vivo we wanted to ascertain the effect of increased eNOS expression during pathologic neovascularization in a model of OIR. In addition, because eNOS-derived peroxynitrite is implicated in contributing to the degenerative phase it was important to determine if eNOS overexpression would exacerbate vaso-obliteration in the hyperoxic phase of the condition between P7 and P12. Indeed, in agreement with this, we found that the eNOS-GFP animals demonstrated a greater loss of retinal vessels at P12 following hyperoxia despite having clear evidence of normal vascular coverage between P7 and P12, as confirmed in the age-matched room air controls. This enhanced obliteration correlated with reduced NOS activity in the absence of BH_4 along with a concomitant enhancement in EC-derived and NOS-dependent DHE fluorescence and NT immunoreactivity. In addition, we also confirmed the presence of NT in the GCL of the avascular retina. As a stable end product of $ONOO^-$ the presence of NT in the site where the vessels of the central retina were once situated suggests a previous $ONOO^-$ mediated insult. Taken together, these findings provide important new in vivo evidence that eNOS is producing superoxide in hyperoxia. This finding has important implications for therapeutic strategies aimed at preventing vascular closure: in addition to decreasing oxidative stress, it will also be necessary to restore NOS function to sufficiently secure vessel integrity in hyperoxia.

In the OIR model, upon return to room air at P12 the rapid development of sustained tissue hypoxia in the avascular inner retina induces the expression of growth factors over the next 5 days, resulting in pathologic angiogenesis characterized by sprouting of newly formed vessels, within the retina and with invasion of the vitreous body. Because this response is most visible at P17 we investigated the effect of eNOS overexpression on pathologic angiogenesis at this time point. We found that despite the exacerbated vaso-obliteration at P12 there was

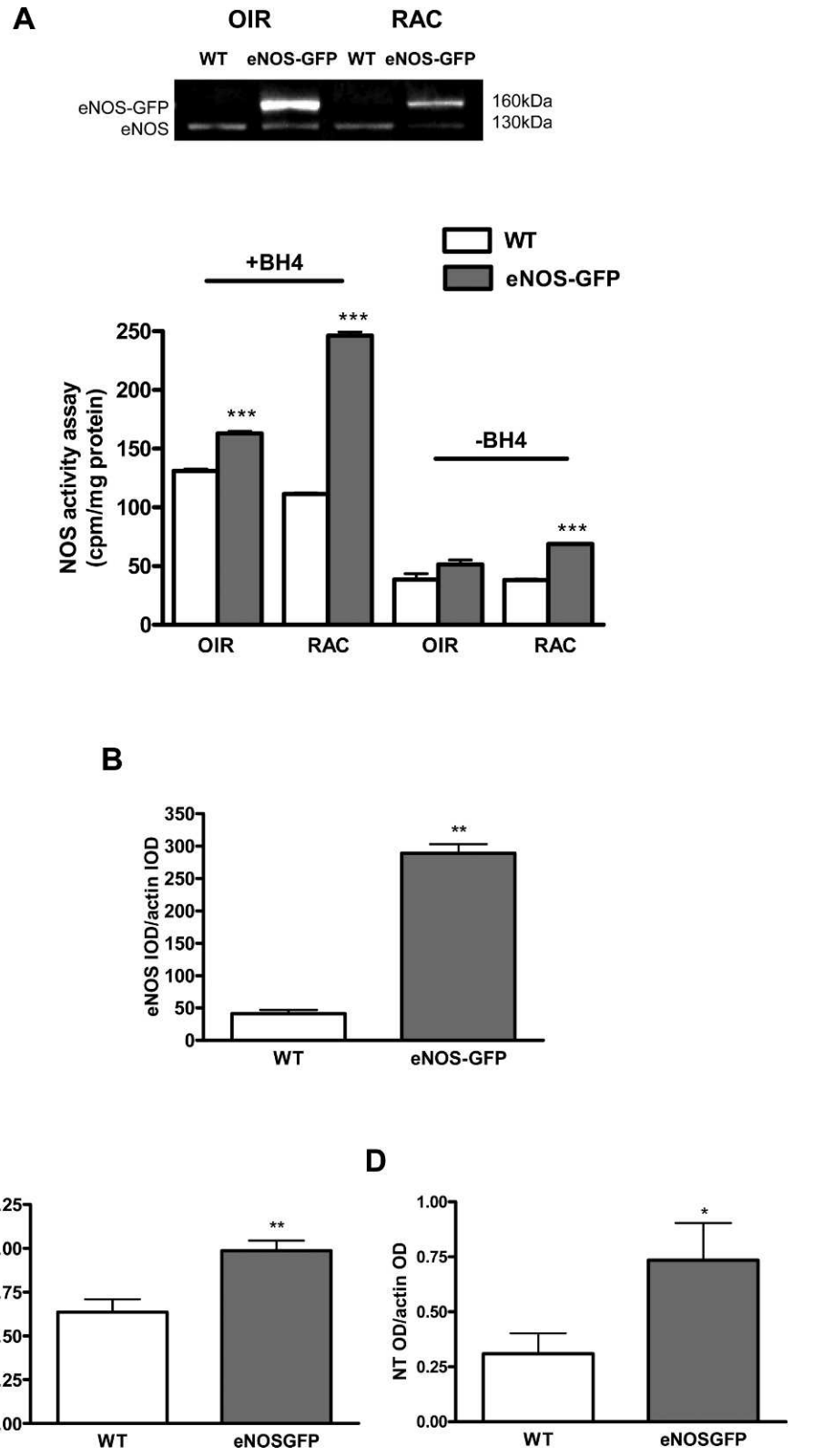

Figure 11. NO and NT levels in P17 retinas following OIR. NO levels were measured from freshly isolated retinas by NOS activity or Griess assay and correlated to the expression of eNOS. (**A**) Western blot of P17 OIR-treated retinas and room air controls (RACs) of the same age. Conversion of radiolabeled arginine to citrulline ($n = 5$ retinas/group) in the presence or absence of BH_4. (**B**) Comparison of total eNOS expression in P17 OIR-treated retinas in WT and eNOS-GFP animals. (**C**) Nitrite accumulation was also measured by Griess assay following stimulation with Ca ionophore ($n = 7$–10 retinas/group). (**D**) Nitrotyrosine immunoreactivity was performed by Western blotting and band intensity quantified. $^{*}P < 0.05$, $^{**}P < 0.01$, $^{***}P < 0.001$.

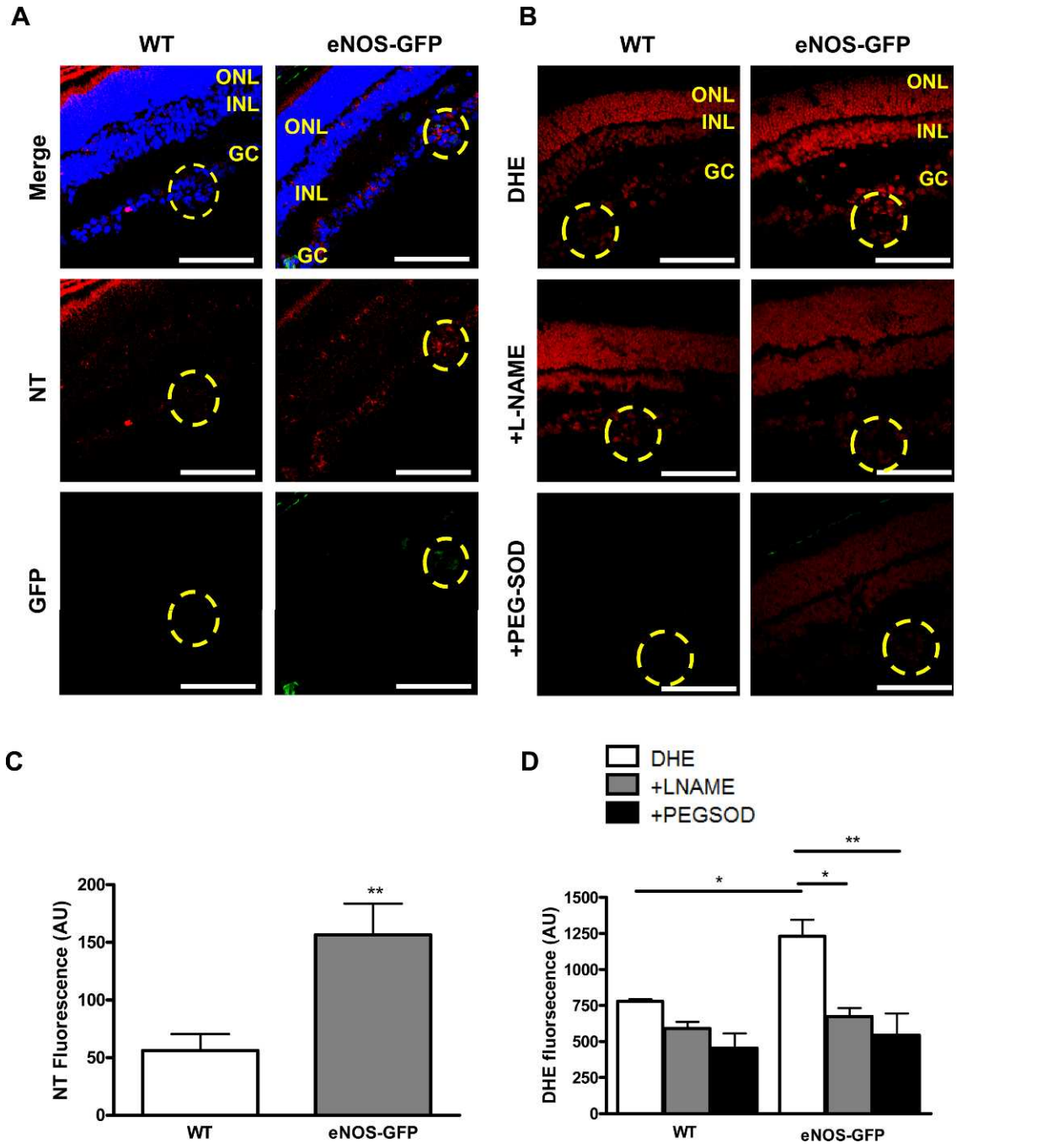

Figure 12. NT immunolocalization and superoxide quantification in neovascular tufts from eNOS-GFP P17 OIR mice. (**A**) Representative images showing NT immunolocalization and (**B**) DHE fluorescence in retinal sections from P17 OIR mice showing increased staining in the neovascular tufts (*outlined area*) in eNOS-GFP mice compared with WT. (**C**) Quantification of NT staining intensity from three sets of eyes from different OIR experiments. (**D**) Superoxide quantification in the presence or absence of L-NAME or PEG-SOD. GCL, ganglion cell layer; INL, inner nuclear layer; ONL, outer nuclear layer. *Scale bars*: 100 μm. $^{*}P < 0.05$, $^{**}P < 0.01$.

a significant increase in vascular growth in the eNOS-GFP animals from P12 to P17 compared with WT animals. This increase in angiogenesis included normal revascularization of the ischemic retina, again with higher vascular density, but also a significant increase in the formation of extraretinal neovascular tufts. Interestingly, the increase in angiogenic drive observed in the eNOS-GFP group compared with controls was much more pronounced post-OIR than occurred during normal physiologic vascular development, suggesting an enhanced role for eNOS. The pathology observed in OIR is complex and it is possible that the effects observed in the vasoobliterative stage could have a significant effect on the later proliferative phase. Therefore, to investigate if the higher revascularization observed in our study was due to the exacerbated vasoobliteration at P12, we quantified VEGF expression at P13 and P17. P13, 24-hour posthyperoxia, is characterized by acute hypoxia and a large increase in hypoxia-induced VEGF production. Therefore, if the larger ischemic area in the eNOS-GFP group were contributing to the enhanced angiogenic drive between P13 and P17, one would expect enhanced

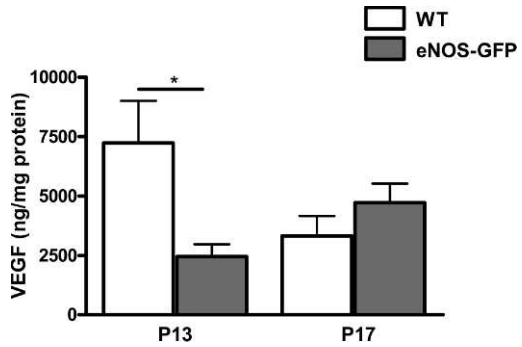

Figure 13. Determination of retinal VEGF levels following OIR. VEGF levels were measured in eNOS-GFP retinal samples at P13 and P17 following OIR by ELISA. Results are of two independent experiments with $n = 3$ retinas per group in each experiment; $^*P < 0.05$.

VEGF production. Yet, this was not the case, given that VEGF was considerably reduced in the eNOS-GFP group compared with the WT controls. Taken together, the VEGF findings and the evidence of an elevated eNOS expression at P12 suggest that the enhanced angiogenic drive from P12 to P13 and P17 was vascular-derived and eNOS-mediated and not a result of enhanced hypoxia. Indeed, this provides further support of a role for eNOS is promoting vascular growth.

We and others have previously shown that in models in which there is accelerated vascular recovery between P13 and P17, the increased intraretinal revascularization occurs in parallel with a decrease in intravitreal NV tuft formation.[7,8] Therefore, in eNOS-GFP animals it was surprising that, in addition to increased normal vessel growth, we also observed an increase in NV tuft formation. It has previously been shown that neovascularization is exacerbated by superoxide production and that this free radical along with peroxynitrite plays an important role in VEGF function acting either directly by enhancing VEGF signaling or indirectly by increasing VEGF production.[43–45] Thus, because we had previously shown that eNOS acts as a source of superoxide in hyperoxia we investigated if this was also the case in the ischemic retina by comparing the amount of NO produced relative to the expression profile of eNOS.[19] We showed that in P17 OIR tissue total eNOS protein expression was 6- to 10-fold higher in the eNOS-GFP animals compared with WT. This large increase in protein expression, however, was not translated into an equivalent increase in NO production or NOS activity, which was only modestly increased (1.5-fold). This was in contrast to the room air controls at the same time point that showed an increase in activity levels comparable to the increase in eNOS protein levels. Performing Western blots from whole retinal lysates showed that there was a global increase in NT formation in the eNOS-GFP retina compared with WT at P17, indicative of increased peroxynitrite formation in the retinas of these animals. Together this suggests that eNOS becomes dysfunctional in the NV phase of OIR, resulting in reduced NO production by eNOS and increased scavenging of NO by superoxide. We investigated this further by quantifying levels of superoxide and other markers of oxidative stress. We found the increased presence of superoxide and nitrotyrosine, localized to neovascular regions associated with an increase in the amount of neovascularization, in accordance with studies from other investigators showing elevated NADPH oxidase activity in these regions.[43] In contrast, here our findings suggest eNOS as a contributor to O_2^- production as a result of eNOS enzymatic dysfunction at the site of neovascularization. It was also interesting to note that in the RAC and adult tissue there were equivalent amounts of eNOS and eNOS-GFP. Post-OIR, however, there was a considerable enhancement of eNOS-GFP expression over that of the endogenous eNOS, suggesting that the human eNOS promoter driving expression of the transgene is more susceptible to hypoxic stimulation than the murine correlate. In the future, it will be interesting to investigate if one of these promoters has a therapeutic advantage over the other for the treatment of ischemic disease.

There are several potential sources of superoxide production in the retina. All three NOS isoforms are expressed in the retina as is NADPH oxidase, which is a significant source of superoxide.[44,45] However, the finding that production of this free radical was localized to the vascular NV regions and the site of eNOS-GFP expression implies eNOS as a possible source. Moreover, the observation that the NOS inhibitor, L-NAME, reduced superoxide production also indicates that NOS is an important source of superoxide in this setting. That we could localize increased superoxide production to the neovascular areas and the fact that the eNOS-GFP mice showed both increased superoxide production and increased neovascularization suggest that the dysfunction of eNOS could be contributing to excessive NV tuft formation. Indeed, this is similar to the situation observed in other vascular diseases. For example, a high ratio of superoxide relative to NO is a contributory factor in disturbed angiogenesis in diabetes.[46–48] Indeed, it is possible that the increase in superoxide compared with NO would have the combined effect of decreasing the amount of NO available to stimulate EC migration, possibly resulting in proliferation at the expense of directional migration as observed in the NV tufts.[12]

A possible cause of the eNOS dysfunction seen in the NV tufts of the eNOS-GFP mice at P17 may be due to insufficiency of the cofactor BH_4, either as a result of increased oxidation caused by augmented superoxide production, or because the quantities of the essential substrate arginine are limiting and do not meet the requirements of the additional eNOS expression.[24,49,50] Next, because we had shown that cofactor insufficiency was partially responsible for eNOS dysfunction during hyperoxia, we wanted to investigate if this was also the case in hypoxia. We found that at P17 post-OIR, in contrast to the effect observed at P12, BH_4 was unable to completely restore NOS activity, suggesting that NOS activity was deficient even in the presence of BH_4. Arginase expression has been shown to be upregulated in the proliferative phase of OIR, which competes with NOS for arginine availability and reduces NOS activity.[30] Here, we compensated for this potentially confounding factor by performing the assays in the presence of an arginase inhibitor. However, it is possible that the inhibitor was unable to suppress the high levels of arginase expressed at P17. Thus, in contrast to the P12 post-OIR retina, both arginine and BH_4 may be limiting in the NV tufts.

Taken together, our results show that eNOS plays an important role in many processes involved in development of the pathology associated with ischemic retinopathy, exerting an influence in both the vasoobliterative and proliferative stages. Importantly, we are the first to show in vivo that because of a relative insufficiency of cofactors that do not meet the needs of overexpressed eNOS, NOS becomes dysfunctional, increases oxidative stress, and exacerbates the effects of hyperoxia on vessel integrity. In parallel, we show that eNOS, in the second proliferative phase of OIR, has important prorepair functions, by enhancing angiogenic growth potential and increasing normal vascular formation and recovery in ischemia. In addition, eNOS overexpression also increases neovascular tuft formation, suggesting that ischemia partially dysregulates the role of eNOS in forming a viable vasculature. Further defining the cause of eNOS dysfunction in hyperoxia and hypoxia may allow for manipulation of eNOS function to

harness its vasoprotective and growth-enhancing potential while also promoting directional revascularization of the ischemic retina**.**

Acknowledgments

The authors thank Adrian Devine for technical assistance.

References

1. Adamis AP, Miller JW, Bernal MT, et al. Increased vascular endothelial growth factor levels in the vitreous of eyes with proliferative diabetic retinopathy. *Am J Ophthalmol*. 1994; 118:445–450.
2. Aiello LP, Avery RL, Arrigg PG, et al. Vascular endothelial growth factor in ocular fluid of patients with diabetic retinopathy and other retinal disorders. *N Engl J Med*. 1994; 331:1480–1487.
3. Pierce E, Avery R, Foley E, Aiello L, Smith L. Vascular endothelial growth factor/vascular permeability factor expression in a mouse model of retinal neovascularization. *Proc Natl Acad Sci U S A*. 1995;92:905–909.
4. Stone J, Itin A, Alon T, et al. Development of retinal vasculature is mediated by hypoxia-induced vascular endothelial growth factor (VEGF) expression by neuroglia. *J Neurosci*. 1995;15: 4738–4747.
5. Ozaki H, Seo M-S, Ozaki K, et al. Blockade of vascular endothelial cell growth factor receptor signaling is sufficient to completely prevent retinal neovascularization. *Am J Pathol*. 2000;156:697–707.
6. Saint-Geniez M, Maharaj ASR, Walshe TE, et al. Endogenous VEGF is required for visual function: evidence for a survival role on Muller cells and photoreceptors. *PLoS ONE*. 2008;3: e3554.
7. Sennlaub F, Courtois Y, Goureau O. Inducible nitric oxide synthase mediates the change from retinal to vitreal neovascularization in ischemic retinopathy. *J Clin Invest*. 2001;107: 717–725.
8. Gardiner TA, Gibson DS, de Gooyer TE, de la Cruz VF, McDonald DM, Stitt AW. Inhibition of tumor necrosis factor-α improves physiological angiogenesis and reduces pathological neovascularization in ischemic retinopathy. *Am J Pathol*. 2005;166:637–644.
9. Papapetropoulos A, García-Cardeña G, Madri J, Sessa W. Nitric oxide production contributes to the angiogenic properties of vascular endothelial growth factor in human endothelial cells. *J Clin Invest*. 1997;100:3131–3139.
10. Ziche M, Morbidelli L, Choudhuri R, et al. Nitric oxide synthase lies downstream from vascular endothelial growth factor-induced but not basic fibroblast growth factor-induced angiogenesis. *J Clin Invest*. 1997;99:2625–2634.
11. Dimmeler S, Fleming I, Fisslthaler B, Hermann C, Busse R, Zeiher AM. Activation of nitric oxide synthase in endothelial cells by Akt-dependent phosphorylation. *Nature*. 1999;399: 601–605.
12. Murohara T, Witzenbichler B, Spyridopoulos I, et al. Role of endothelial nitric oxide synthase in endothelial cell migration. *Arterioscler Thromb Vasc Biol*. 1999;19:1156–1161.
13. Brooks SE, Gu X, Samuel S, et al. Reduced severity of oxygen-induced retinopathy in eNOS-deficient mice. *Invest Ophthalmol Vis Sci*. 2001;42:222–228.
14. Ando A, Yang A, Mori K, et al. Nitric oxide is proangiogenic in the retina and choroid. *J Cell Physiol*. 2002;191:116–124.
15. Amano K, Matsubara H, Iba O, et al. Enhancement of ischemia-induced angiogenesis by eNOS overexpression. *Hypertension*. 2003;41:156–162.
16. Namba T, Koike H, Murakami K, et al. Angiogenesis induced by endothelial nitric oxide synthase gene through vascular endothelial growth factor expression in a rat hindlimb ischemia model. *Circulation*. 2003;108:2250–2257.
17. Stone J. Development of retinal vasculature is mediated by hypoxia-induced endothelial growth factor expression by neuroglia. *J Neurosci*. 1995;15:4738–4747.
18. Gerhardt H, Golding M, Fruttiger M, et al. VEGF guides angiogenic sprouting utilizing endothelial tip cell filopodia. *J Cell Biol*. 2003;161:1163–1177.
19. Xia Y, Tsai AL, Berka V, Zweier JL. Superoxide generation from endothelial nitric-oxide synthase. A Ca2+/calmodulin-dependent and tetrahydrobiopterin regulatory process. *J Biol Chem*. 1998;273:25804–25808.
20. Hardy P, Beauchamp M, Sennlaub F, et al. New insights into the retinal circulation: inflammatory lipid mediators in ischemic retinopathy. *Prostaglandins Leukot Essent Fatty Acids*. 2005; 72:301–325.
21. Saito Y, Uppal A, Byfield G, Budd S, Hartnett ME. Activated NAD(P)H oxidase from supplemental oxygen induces neovascularization independent of VEGF in retinopathy of prematurity model. *Invest Ophthalmol Vis Sci*. 2008;49:1591–1598.
22. Uno K, Merges CA, Grebe R, Lutty GA, Prow TW. Hyperoxia inhibits several critical aspects of vascular development. *Dev Dyn*. 2007;236:981–990.
23. Kermorvant-Duchemin E, Sennlaub F, Sirinyan M, et al. Transarachidonic acids generated during nitrative stress induce a thrombospondin-1-dependent microvascular degeneration. *Nat Med*. 2005;11:1339–1345.
24. Laursen JB, Somers M, Kurz S, et al. Endothelial regulation of vasomotion in apoE-deficient mice: implications for interactions between peroxynitrite and tetrahydrobiopterin. *Circulation*. 2001;103:1282–1288.
25. Ozaki M, Kawashima S, Yamashita T, et al. Overexpression of endothelial nitric oxide synthase accelerates atherosclerotic lesion formation in apoE-deficient mice. *J Clin Invest*. 2002; 110:331–340.
26. van Haperen R, de Waard M, van Deel E, et al. Reduction of blood pressure, plasma cholesterol, and atherosclerosis by elevated endothelial nitric oxide. *J Biol Chem*. 2002;277: 48803–48807.
27. van Haperen R, Cheng C, Mees BME, et al. Functional expression of endothelial nitric oxide synthase fused to green fluorescent protein in transgenic mice. *Am J Pathol*. 2003; 163:1677–1686.
28. Cheng C, van Haperen R, de Waard M, et al. Shear stress affects the intracellular distribution of eNOS: direct demonstration by a novel in vivo technique. *Blood*. 2005;106:3691–3698.
29. Smith L, Wesolowski E, McLellan A, et al. Oxygen-induced retinopathy in the mouse. *Invest Ophthalmol Vis Sci*. 1994;35: 101–111.
30. Stevenson L, Matesanz N, Colhoun L, et al. Reduced nitro-oxidative stress and neural cell death suggests a protective role for microglial cells in TNF–/– mice in ischemic retinopathy. *Invest Ophthalmol Vis Sc*. 2010;51:3291–3299.
31. Matesanz N, Park G, McAllister H, et al. Docosahexaenoic acid improves the nitroso-redox balance and reduces VEGF mediated angiogenic signaling in microvascular endothelial cells. *Invest Ophthalmol Vis Sci*. 2010;51:6815–6825.
32. Suchting S, Heal P, Tahtis K, Stewart LM, Bicknell R. Soluble Robo4 receptor inhibits in vivo angiogenesis and endothelial cell migration. *FASEB J*. 2004;19:121–123.
33. Garcia-Cardena G, Martasek P, Masters BS, et al. Dissecting the interaction between nitric oxide synthase (NOS) and caveolin. Functional significance of the NOS caveolin binding domain in vivo. *J Biol Chem*. 1997;272:25437–25440.
34. Michel JB, Feron O, Sacks D, Michel T. Reciprocal regulation of endothelial nitric-oxide synthase by Ca2+-calmodulin and caveolin. *J Biol Chem*. 1997;272:15583–15586.

35. Garcia-Cardena G, Oh P, Liu JW, Schnitzer JE, Sessa WC. Targeting of nitric oxide synthase to endothelial cell caveolae via palmitoylation—implications for nitric oxide signaling. *Proc Natl Acad Sci U S A*. 1996;93:6448–6453.
36. Ju H, Zou R, Venema VJ, Venema RC. Direct interaction of endothelial nitric-oxide synthase and caveolin-1 inhibits synthase activity. *J Biol Chem*. 1997;272:18522–18525.
37. Fulton D, Gratton J-P, McCabe TJ, et al. Regulation of endothelium-derived nitric oxide production by the protein kinase Akt. *Nature*. 1999;399:597–601.
38. McDonald D, Alp N, Channon K. Functional comparison of the endothelial nitric oxide synthase Glu298Asp polymorphic variants in human endothelial cells. *Pharmacogenetics*. 2004; 14:831–839.
39. Chan-Ling T, Gock B, Stone J. The effect of oxygen on vasoformative cell division. Evidence that "physiological hypoxia" is the stimulus for normal retinal vasculogenesis. *Invest Ophthalmol Vis Sci*. 1995;36:1201–1214.
40. Fukumura D, Gohongi T, Kadambi A, et al. Predominant role of endothelial nitric oxide synthase in vascular endothelial growth factor-induced angiogenesis and vascular permeability. *Proc Natl Acad Sci U S A*. 2001;98:2604–2609.
41. Kashiwagi S, Izumi Y, Gohongi T, et al. NO mediates mural cell recruitment and vessel morphogenesis in murine melanomas and tissue-engineered blood vessels. *J Clin Invest*. 2005;115: 1816–1827.
42. Parsons-Wingerter P, Chandrasekharan UM, McKay TL, et al. A VEGF165-induced phenotypic switch from increased vessel density to increased vessel diameter and increased endothelial NOS activity. *Microvasc Res*. 2006;72:91–100.
43. Ushio-Fukai M, Tang Y, Fukai T, et al. Novel role of gp91phox-containing NAD(P)H oxidase in vascular endothelial growth factor-induced signaling and angiogenesis. *Circ Res*. 2002;91: 1160–1167.
44. Al-Shabrawey M, Bartoli M, El-Remessy AB, et al. Inhibition of NAD(P)H oxidase activity blocks vascular endothelial growth factor overexpression and neovascularization during ischemic retinopathy. *Am J Pathol*. 2005;167:599–607.
45. El-Remessy AB, Al-Shabrawey M, Platt DH, et al. Peroxynitrite mediates VEGF's angiogenic signal and function via a nitration-independent mechanism in endothelial cells. *Am J Pathol*. 2007;21:2528–2539.
46. Ebrahimian TG, Heymes C, You D, et al. NADPH oxidase-derived overproduction of reactive oxygen species impairs postischemic neovascularization in mice with type 1 diabetes. *Am J Pathol*. 2006;169:719–728.
47. Li Calzi S, Purich DL, Chang KH, et al. Carbon monoxide and nitric oxide mediate cytoskeletal reorganization in microvascular cells via vasodilator-stimulated phosphoprotein phosphorylation. *Diabetes*. 2008;57:2488–2494.
48. Haddad P, Dussault S, Groleau J, et al. Nox2-containing NADPH oxidase deficiency confers protection from hindlimb ischemia in conditions of increased oxidative stress. *Arterioscler Thromb Vasc Biol*. 2009;29:1522–1528.
49. Bendall JK, Alp NJ, Warrick N, et al. Stoichiometric relationships between endothelial tetrahydrobiopterin, endothelial NO synthase (eNOS) activity, and eNOS coupling in vivo: insights from transgenic mice with endothelial-targeted GTP cyclohydrolase 1 and eNOS overexpression. *Circ Res*. 2005;97: 864–871.
50. Takaya T, Hirata K-i, Yamashita T, et al. A specific role for eNOS-derived reactive oxygen species in atherosclerosis progression. *Arterioscler Thromb Vasc Biol*. 2007;27:1632–1637.